Analyst

Accepted Manuscript

ROYAL SOCIETY OF CHEMISTRY

www.rsc.org/analyst

Analyst

RSCPublishing

PAPER

In-line microfluidic integration of photonic crystal fibre as a highly sensitive refractometer

Cite this: DOI: 10.1039/x0xx00000x

Chuang Wu,[a] Ming-Leung Vincent Tse,[b] Zhengyong Liu,[b] Bai-Ou Guan,*[a] A. Ping Zhang,[b] Chao Lu,[c] and Hwa-Yaw Tam*[b]

Photonic crystal fibres appear to be an ideal platform for the realisation of novel optofluidic devices and sensors due to the waveguide nature and the microstructured architecture of them. In this paper, we present the fabrication and characterisation of an in-line photonic crystal fibre microfluidic refractometer enabled by a C-shaped fibre. The C-shaped fibre spliced in-between the photonic crystal fibre and the single-mode fibre allows simultaneous in-line optical signal delivery and analyte fluid feeding. Through an arc discharge pre-treatment technique, we successfully achieve selective exploitation of only the central two channels of the photonic crystal fibre for microfluidic sensing. After constructing a Sagnac interferometer, a highly sensitive refractometer with sensitivity of 8699 nm/RIU and was achieved experimentally; this agrees very well with the theoretical value of 8675 nm/RIU. As a demonstration for label-free optical sensing application, the refractometer was used to measure the concentration of NaCl solution with a sensitivity of 15.08 nm/(1wt%) and detection limit of 2.3×10^{-3}wt% (23 ppm).

Received 24th July 2014
Accepted 00th July 2014

DOI: 10.1039/x0xx00000x

www.rsc.org/an

Introduction

Optical fibre refractometers have received extensive interest in the context of label-free optical sensing of chemical and biological samples because they are compact in size, immune to electromagnetic interference, inexpensive to mass produce, and easy for signal delivery.[1] Label-free sensing does not require the sample to be marked with fluorescent dyes but rather relies on the detection of tiny refractive index changes induced by chemical reactions or biological bonding events.[2] In recent years, many fibre-optic refractometers based on various principles have been reported, such as optical fiber gratings,[3-5] optical fibre interferometers,[6-8] and optical fibre surface plasmon resonance sensor.[9] However, the sensitivities of these refractometers are usually no better than several hundred nanometers per refractive index unit (nm/RIU) with detection limit of 10^{-2} to 10^{-4}. Further effort to improve the refractive index sensitivity is required to achieve better performance of label-free optical sensing.

[a] *Institute of Photonics Technology, Jinan University, Guangzhou 510632, China. Email: tguanbo@jnu.edu.cn*
[b] *Department of Electrical Engineering, The Hong Kong Polytechnic University, Hong Kong, China. Email: hwa-yaw.tam@polyu.edu.hk*
[c] *Department of Electronic and Information Engineering, The Hong Kong Polytechnic University, Hong Kong, China.*

Optofluidics is an emerging field that integrates optics and microfluidics.[10] It provides new freedom to both fields and permits the realisation of novel optical waveguides, devices, and sensors.[11-13] For instance, Yang *et al.* demonstrated large angle light bending and tuning in an optofluidic waveguide based on transformation optics.[14,15] Song and Psaltis realised a pneumatically tunable optofluidic switch for fast response on-chip light routing.[16] Testa and Bernini implemented a tunable liquid optical fibre with a 3D hydrodynamic focusing scheme.[17] At the same time, significant efforts have been devoted to developing novel optofluidic refractometers employing various schemes, such as optical ring resonator with a silica capillary,[18] surface-enhanced Raman scattering detection with a capillary array,[19] on-chip Fabry–Pérot interferometer[20] and Mach-Zehnder interferometers,[21-23] and hollow core anti-resonant reflecting optical waveguide.[24]

Photonic crystal fibres (PCFs),[25] in which periodic air holes running along the axial direction, appear to be an ideal platform for the realisation of optofluidic devices due to the waveguide nature and the microstructred architecture found within them.[26-28] The micron-sized air holes of the PCFs are inherent microfluidic channels allowing analyte fluids to pass through. The optical properties of PCFs such as transmission loss, modal effective index, scattering, and dispersion are highly dependent on the refractive index of the fluids occupying the air hole channels. This enables a lot of microfluidic refractometers, such

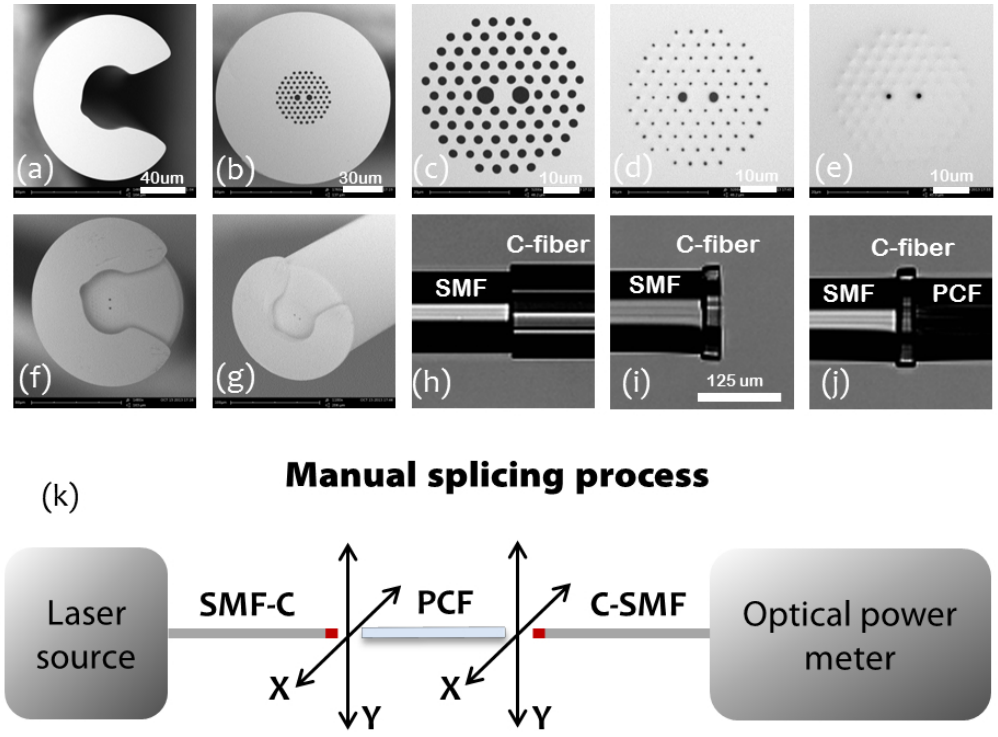

Fig. 1 (a) & (b) SEM photos of the cross sections of the C-shaped fibre and the PM-PCF, respectively. (c) – (e) SEM photos for the evolution of air hole structure on the facet of the PM-PCF during arc discharge pre-treatment: without arc discharge, arc charge once, arc charge twice, respectively. Only the central two large air holes remained open. (f) & (g) PM-PCF with an ultrathin piece of C-shaped fiber attached on its end. (h) - (j) Side view images of optical fibres during fusion splicing. (k) Schematic of the manual splicing process. The red dots represent ultrathin pieces of C-shaped fibres on the end of SMF.

as those based on spectroscopy in hollow-core PCFs,[29-35] fibre gratings in solid-core PCFs,[36-38] analyte waveguide formed directional coupler,[39] modal interferometer,[40] and SERS detection.[41] The PCF-based microfluidic refractometers have more flexibility in sensor design over other counterparts. Hence it is easy to achieve higher sensitivity and lower detection limit.

To date, there are mainly two approaches to couple light in and out of PCFs for signal delivery. One is to directly splice the PCFs to normal single-mode fibres (SMF);[36-38] the other uses free space optics.[29-35] For the former, it is difficult to reuse the senor; for the latter, the use of adjustable stages and bulky optics makes the system complicated. In order to realise in-line access to the air holes of the PCFs, some groups drill holes on the side of PCFs with the fs-laser micromachining system.[42-44] However, it requires high-quality femto-second laser beam and accurate positioning devices, rendering the devices expensive to produce. Recently, our group developed a simple and cost-effective solution to fabricate in-line PCF microfluidic devices with the help of a C-shaped fibre.[45]

In this paper, we report the fabrication and characterisation of an in-line photonic crystal fibre microfluidic refractometer enabled by a C-shaped fiber. Ultrathin piece of C-shaped fibres spliced in-between the photonic crystal fibre and the single-mode fibres allow simultaneous in-line optical signal delivery and analyte fluid feeding. Using an arc discharge pre-treatment technique, we achieve selective exploitation of only the central two air hole channels of the photonic crystal fibre for advanced sensing, improving the sensitivity by 70% compared with the case of employing all the air hole channels.[45] Based on a Sagnac interferometer configuration, a high sensitivity of 8699 nm/RIU for refractive index around 1.33 was achieved in the experiment, which, notably, agrees superbly with the theoretical value of 8675 nm/RIU. As a demonstration for label-free optical sensing application, the refractometer was used to measure the concentration of NaCl solution with a sensitivity of 15.08 nm/(1wt%) and detection limit of 2.3×10^{-3}wt% (23 ppm).

Methods

Materials and fabrication

The C-shaped fibre was fabricated in-house using an optical fibre drawing tower (NEXTROM© OFC20). Firstly a silica tube with inner diameter of 4 mm and outer diameter of 12 mm was machined to create a lateral slot along the axial direction, resulting in a C-shaped preform. Then the preform was drawn into C-shaped fibre with outer diameter of 145 μm and effective inner diameter of 48 μm. During drawing, the oven of the tower was set to a relatively low temperature of 1890 °C to maintain the cross-sectional shape of the fibre. Fig. 1 (a) shows the SEM photo of the cross section of the fabricated C-shaped fiber.

The polarisation-maintaining photonic crystal fibre (PM-PCF) was purchased from NKT Photonics company (Product Code: PM-1550-01). Fig. 1 (b) shows the SEM photo of the cross section of the PM-PCF. It has small air holes with diameter of

2.25 μm and hole-to-hole pitch of 4.33 μm; the two large air holes locating at the opposite sides of the fiber core are 4.20 μm × 4.60 μm in size, resulting in a noncircular core with a modal birefringence of ~10^{-4}.

In order to selectively exploit only the central two large air hole channels for advanced refractive index sensing, we treated both end facets of the PM-PCF by proper arc discharges before splicing them to the C-shaped fibre, so that the small air hole voids near the surface were sealed while the large air hole voids remained open.[46] The arc discharge parameters are as follow: the offset between the fiber end and the electrodes in z-direction is 5 μm; the arc discharge intensity is 20 units defined by the splicer; arc discharge duration per time is 200 ms; the arc discharge was performed twice. Fig. 1 (c) – (e) show the SEM photos for the evolution of air hole shrinkage on the facet of the PM-PCF during arc discharge treatment. We find that all the small air holes are completely collapsed, while the two large air holes remains open with a diameter of ~1 μm. The length of the PM-PCF used in the experiment is 11.2 mm.

The fabrication process of the in-line microfluidic device is quite simple. Firstly, we splice an SMF and a piece of C-shaped fibre, as shown in fig. 1 (h). Because the C-shaped fibre is noncircular, manual splicing program is needed. Then, we cut the C-shaped fibre to ~20 μm with the help of a microscope with 100 times amplification. The resultant SMF-C part is shown in fig. 1 (i). Following the same procedure, we produce the other C-SMF part. Finally, we splice both ends of the PM-PCF to the SMF-C and C-SMF parts, as shown in fig. 1 (j), using a manual splicing program to achieve splicing joints with low optical coupling loss and good mechanical strength.[47] Figure 1 (k) shows the schematic of the manual splicing process. A laser source (Santec TSL-210) and a fibre optic power meter (ILXLightwave FPM-8210H) were used to monitor the optical transmission loss and help alignment of the fibres during splicing. The model of the fusion splicer and the optical fibre cutter used in the experiment are FITEL S177A and S325, respectively. The total transmission loss of the fabricated SMF-C-PCF-C-SMF microfluidic device was 12.3 dB.

Principle of operation

An optical fibre Sagnac interferometer consists of a broadband light source, an optical spectrum analyser (OSA), and a 3 dB coupler with its two other arms connected with a piece of high-birefringence fibre, forming a closed Sagnac loop, as shown in fig. 2 (a). A polarisation controller is inserted in the fiber loop to adjust polarisation states of the light waves for optimisation of the intensity contrast of the output spectrum. A broad band light launches into the fiber loop through arm 1 of the coupler, and the light wave is equally split into arms 3 and 4 of the coupler, resulting in the two counter-propagating light waves within the fiber loop. Due to the existence of the birefringence in the fibre loop, when the two light waves recombine at arm 2 of the 3 dB coupler, they experiences phase difference and produces an interference spectrum that can be measured by the OSA. The phase difference is related to the birefringence and the length of the PM-PCF.

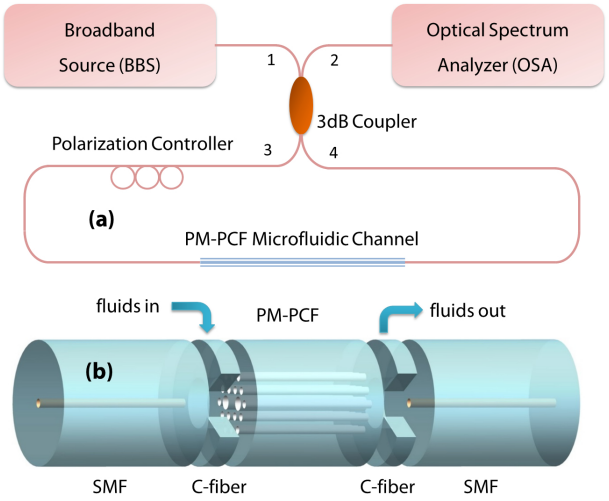

Fig. 2 (a) Schematic of the PM-PCF based Sagnac interferometer. (b) Schematic of the SMF-C-PCF-C-SMF microfluidic device.

Figure 2 (b) shows the schematic of the proposed in-line PM-PCF microfluidic refractometer. Ultrathin pieces of C-shaped fibre are spliced in-between the PM-PCF and SMF. This device allows simultaneous in-line optical signal delivery and analyte fluids feeding to the PM-PCF: the central hollow area of the C-shaped fibre transmits light wave, and the side-opening of the C-shaped fibre provides inlet and outlet for fluids.

When the analyte fluid fills the air hole channels of the PM-PCF, it modifies the refractive index distribution over the cross section of PM-PCF and thus changes the effective indices of the guided modes of it. Consequently, the birefringence of the PM-PCF changes and the interference spectrum shifts. Thus, the refractive index of the analyte can be unambiguously determined by tracking the wavelength shift of the interference spectrum.

According to the theory of polarimetric interferometry, the transmission spectrum of the Sagnac interferometer equals an approximately periodic function of wavelength and is described by[48]

$$T = \frac{1}{2}\left(1 - \cos\frac{2\pi B(\lambda, n_a)L}{\lambda}\right), \quad (1)$$

where λ is the free space wavelength, n_a is the refractive index of the analyte filled in the air hole channels of the PM-PCF, and L is the length of the PM-PCF. The phase modal birefringence B and group modal birefringence G of the PM-PCF are defined by

$$\begin{aligned} B(\lambda) &= n_{eff}^{slow}(\lambda) - n_{eff}^{fast}(\lambda) \\ G(\lambda) &= B(\lambda) - \lambda\, dB(\lambda)/d\lambda \end{aligned}, \quad (2)$$

where $n_{eff}^{slow}(\lambda)$ and $n_{eff}^{fast}(\lambda)$ are the effective indices of the two orthogonal polarized modes of the PM-PCF. Transmission dips appear when the phase difference satisfies

$$\frac{2\pi B(\lambda, n_a)L}{\lambda} = 2m\pi, \quad (3)$$

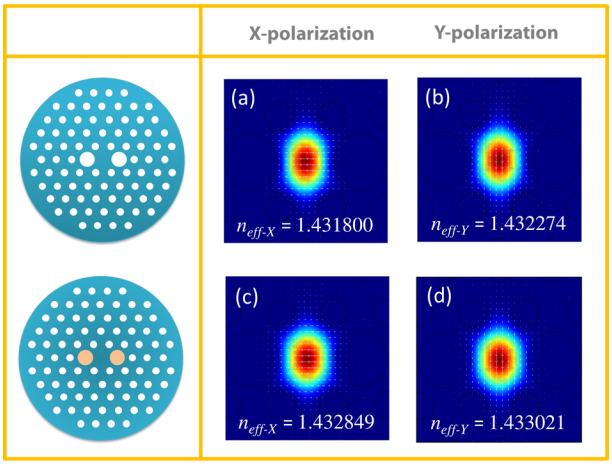

Fig. 3 The simulated mode fields and effective indices of the PM-PCF before (n_a = 1.00) and after (n_a = 1.33) water filling. For the pictures in the first column, the light-blue, the white, and the orange colours represent silica material, air holes, and analyte channels, respectively.

where m is an integer. Then we calculate the derivative of two sides of equation (3) with respect to n_a and take equation (2) into consideration. By doing this, we deduce that the refractive index sensitivity is governed by the following equation:

$$S = \frac{d\lambda}{dn_a} = \frac{\lambda}{G(\lambda, n_a)} \frac{\partial B(\lambda, n_a)}{\partial n_a}. \quad (4)$$

For two adjacent transmission dips of the interference spectrum with a wavelength spacing $\Delta\lambda$, the accumulated phase difference over $\Delta\lambda$ is $\pm 2\pi$, from which we deduce that the absolute value of G is determined as follow

$$|G| = \lambda^2 / (\Delta\lambda L). \quad (5)$$

Numerical simulation

The modal effective index and the birefringence of the PM-PCF were simulated based on a finite element method (FEM) with commercially available COMSOL software. The perpendicular wave module of the software was used to solve wave equations and calculated the effective indices of the guided modes in the PM-PCF. In order to study the dispersion characteristics we did wavelength scanning, i.e., performing simulations at different wavelengths. Thus we achieve the value of B as a function of λ. Next we do the third-order polynomial fitting for B and λ so as to calculate the derivative of B with respect to λ. And then the value of G was calculated according to equation (2). Fig. 3 shows the simulated mode fields and effective indices at the wavelength of 1575 nm for PM-PCF filled with air and analyte, respectively. The material dispersion of silica and water were taken into consideration according to the Sellmeier equation.[49]

In order to simulate the theoretical value of the refractive index sensitivity of the sensor, we set n_a to be different values and repeated the previous wavelength scanning process at each value of n_a. Hence we obtained the curves of B as a function of λ at different n_a values, i.e., a quasi-two-dimensional map of $B(\lambda, n_a)$. By substituting the obtained $B(\lambda, n_a)$ to equation (1), the simulated output spectra for different n_a values can be obtained. Then the refractive index sensitivity was calculated

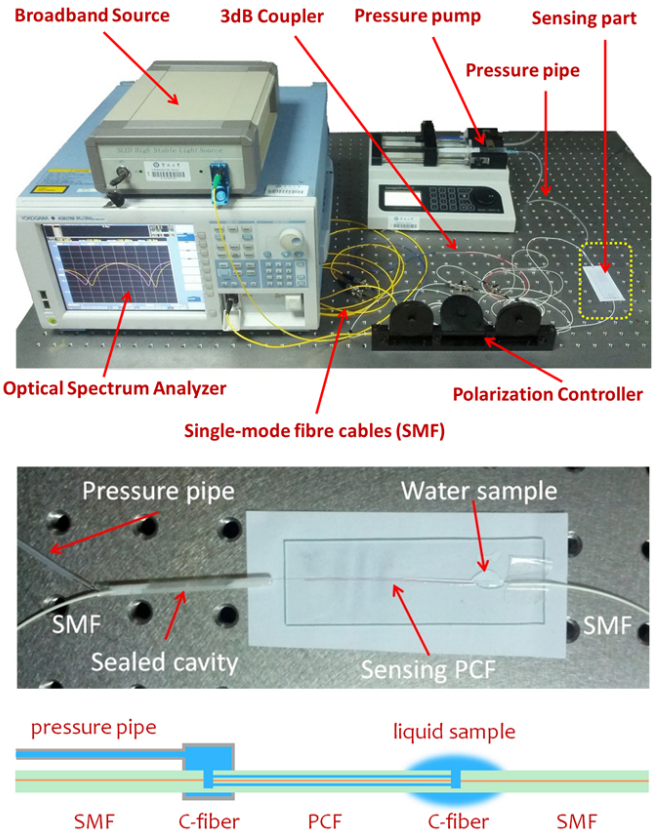

Fig. 4 The top photo shows the experimental setup. The middle photo shows the enlarged photo of the sensing part. The bottom is the schematic of the sensing part. The PCF was labelled in red so that it is visible for taking photo.

by tracking the wavelength shift of the spectrum. Alternatively, , one can also obtain the value of $\partial B / \partial n_a$ from those simulation results, and then calculate the sensitivity by use of equation (4). These two methods give the same sensitivity since they are both deduced from equation (1).

Characterisation

Experiments were carried out to measure the refractive index sensitivity of the fabricated microfluidic refractometer. The refractive index around 1.33 is of most interest for biological sensing applications, because most bio-events take place in aqueous environments. Thus we use deionized (DI) water as the analyte. One of the SMF-C-PCF joint was immersed in a bath filled with DI water. Due to capillary action, the DI water automatically fills the two microfluidic channels of the PM-PCF.[50] Since the water-filled PM-PCF has smaller value of G, the wavelength spacing of the interference spectrum became larger and larger during water filling. After 5 minutes, the spectral evolution stopped, indicating the water was fully filled over the entire length of the PM-PCF.

The PM-PCF Sagnac interferometer itself is intrinsically temperature insensitive because the PM-PCF is made entirely of silica and its birefringence does not change with temperature variation.[51] Therefore, one can characterize the refractive index response of the sensor by varying the temperature to tune the refractive index of the water in the air hole channels of the PM-

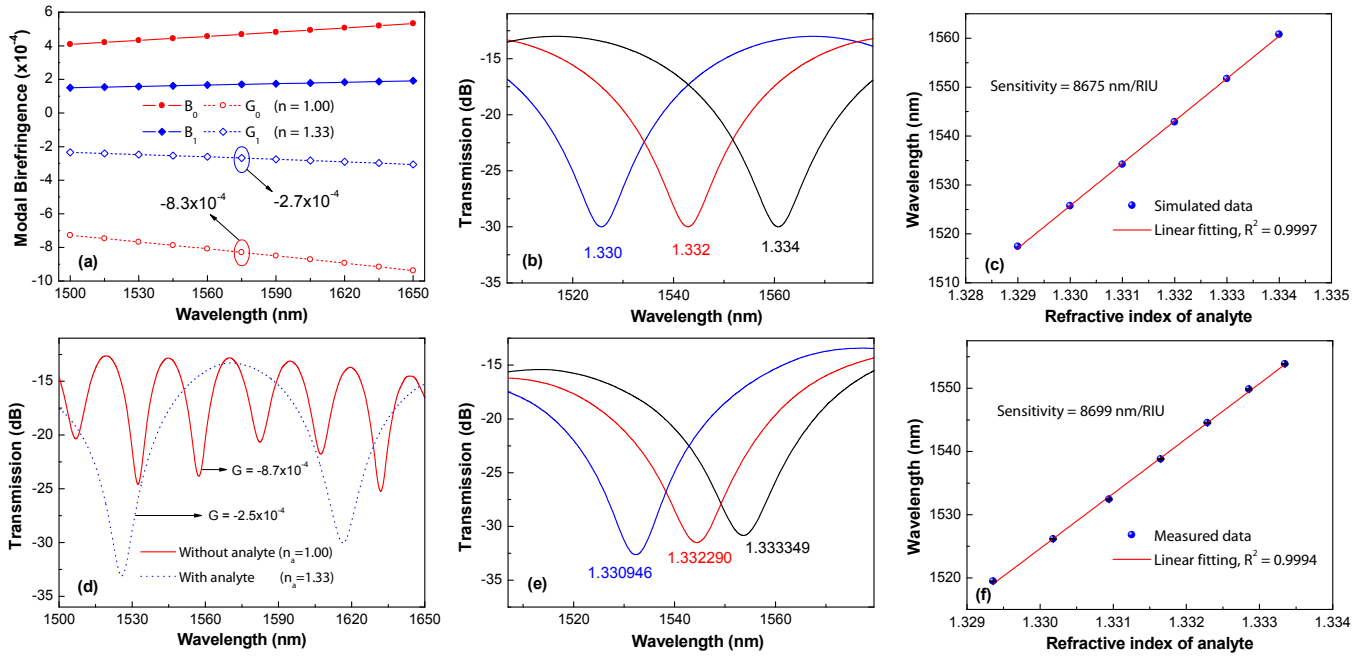

Fig. 5 (a) Simulated modal birefringence of the PM-PCF as a function of wavelength, before and after water filled. (b) Simulated spectral shift for different values of analyte refractive index. (c) Simulated wavelength shift as a function of analyte refractive index. (d) Experimental spectra achieved before and after water filled. (e) Experimental spectral shift for different values of analyte refractive index. (f) Experimental wavelength shift as a function of analyte refractive index. Error bar is standard deviation (S.D.) value.

PCF. In other words, different temperatures correspond to different values of refractive index of analyte applied to the sensor.[49] A FLUKE 52II thermometer with accuracy of 0.1 ºC was used to monitor the change of water temperature. Experimental data were collected in a step of 5 ºC.

Fig. 4 shows the photo of our experimental setup. As can be seen from it, one of SMF-C-PCF joint was sealed in a pressure tube connected to an injection syringe for pressure adjustment; the other SMF-C-PCF joint was immerged in a liquid drop. The injection syringe was fixed on an electrically controlled moving stage to produce a uniform pressure. When pulling the plunge of the injection syringe, it produces a vacuum pressure in the tube that attracts the fluids fill in the PCF. When the pulling distance is set to 10 mm, it takes 1 minute for water to fill the entire length of the 11.2 mm long PCF. The filling speed also depends on the material properties of the liquid, such as its density and viscosity. Oppositely, a compressive pressure can be produced in the pressure tube by pushing the plunge of the injection syringe, which can exclude the liquids out of the PCF. The purge process also takes about 1 minute when the pushing distance is set to 10 mm. Consequently, the sensor can be used multiple times. The bare PCF has a diameter of 125 μm (the same as a normal optical fibre). The two microfluidic channels used for sensing have a diameter of only 4.3 μm, and they are surrounded by 4 rings of air hole voids in the cladding (see fig. 1). Even under a microscope, the microfluidic channels are not transversely visible due to small size and complex structure of them. As a result, we observe the optical spectrum to identify whether the PCF is fully filled. The optical spectrum stops evolution and becomes stable after the PCF is fully filled.

Results and discussion

Theoretical refractive index sensitivity

The simulation results of B and G as a function of wavelength for air-filled (n_a = 1.00) and water-filled (n_a = 1.33) PM-PCF are plotted in fig. 5 (a). It is observed that the values of the group birefringence of the PM-PCF at the wavelength of 1575 nm before and after water filled are -8.3×10^{-4} and -2.7×10^{-4}, respectively. By substituting the obtained $B(\lambda, n_a)$ to equation (1), the simulated output spectra for different n_a values was obtained and plotted in fig. 5 (b). Then we tracked the shifting of the spectral dip in fig. 4 (b), and achieved wavelength shift as a function of the refractive index of analyte as shown in fig. 4 (c). Through linear fitting, the refractive index sensitivity was calculated to be 8675 nm/RIU with good linearity of 0.9997.

In equation (4), both terms of G and $\partial B/\partial n_a$ have negative values, resulting in positive value of refractive index sensitivity. This indicates that the spectrum red shifts with increase in n_a, which is consistent with fig. 4 (a) and (b). In the simulation, the unflatness of the broadband light source and the wavelength dependent absorption loss of water were not considered, thus the achieved spectra dips exhibit uniform power.

Measured refractive index sensitivity

Fig. 5 (d) shows the measured spectra of the sensor filled with air (n_a = 1.00) and water (n_a = 1.33). According to equation (5), the experimental value of G was calculated to be -8.7×10^{-4} and -2.5×10^{-4} at the wavelength of 1575 nm for the two cases, respectively, both of which agree well with the theoretical

values presented hereinbefore. Fig. 4 (e) shows the measured We find that the spectrum shifted to longer wavelength with increase in n_a, which is consistent with the theoretical result shown fig. 4 (b). By tracking the wavelength shift in fig. 4 (e), we achieve refractive index response curve shown in fig. 4 (f). Linear fitting of the data indicated very high sensitivity of 8699 nm/RIU with good linearity of 0.9994. Notably, the measured value of 8699 nm/RIU matches perfectly with the theoretical value of 8675 nm/RIU. This proves that the theoretical model we applied is effective and convincing. It is also observed that the optical power of the spectral dip changed during shifting. This is mainly due to two reasons: 1) the optical power of the light source is not flat over the whole wavelength range; 2) part of the optical field (see fig. 3) penetrates into the water channel, and the absorption loss of water is wavelength dependent. As a result, when the spectrum dip shifts to different wavelengths, it suffers different losses and exhibits different strengths. Since the sensing relies on the detection of wavelength shift, the optical power fluctuation does not affect the result. This is its advantage over the fluoresce-based intensity detection sensors.

The two microfluidic channels used for sensing have length of 11.2 mm and diameter of 4.3 μm, it can be calculated that the minimum volume required for analysis is as small as 3.1 nL. In the experiment, the AQ6370 OSA with resolution of 0.02 nm was used to measure the interference spectrum. The full width at half maximum (FWHM) of the transmission notch is 4.9 nm. The associated refractive index detection limit is calculated to be 4.0×10^{-6} RIU according to the formula by White and Fan.[52] Providing an optical spectrum analyzer with higher resolution, the detection limit of the refractometer can be further improved. The measurement range of the refractometer is governed by the free spectral range (FSR) of the interference spectrum. FSR is defined by the wavelength spacing of two adjacent notches in the spectrum. For our refractometer, the FSR is 87.8 nm, thus the measurement range is 87.8 nm / 8699 (nm/RIU) = 0.01 RIU. Equation (5) indicates that the FSR is inversely proportional to the length of the PM-PCF. Thus, the measurement range will be larger if shorter PM-PCF is used. However, larger FSR usually leads to broader FWHM, which depresses the detection limit of the refractometer.

It is reported that a microfluidic Fabry-Perot interferometer has a RI sensitivity of ~1100 nm/RIU;[20] a long-period grating (LPG) in a PCF exhibits sensitivities of 400~1500 nm/RIU, depending of the order of cladding mode used;[38] a fiber Bragg grating in a three-hole microstructred fiber has a sensitivity less than 100 nm/RIU;[36] the sensitivity of our sensor (8700 nm/RIU) is much better than these ones. Particularly, a directional coupler-based PCF refractometer through selectively filling one air hole in the second ring of the cladding achieved sensitivity as high as 30100 nm/RIU.[39] This sensor can only measure RI higher than the background, i.e., larger than 1.444. However, most bio-events happen in aqueous environments whose RI is around 1.333. For these applications, our sensor works better.

Measurement of concentration of NaCl solution

The concentration of NaCl solution is also known as salinity. Accurate measurement of salinity plays an important role in many areas, such as manufacturing process control, protection of ecosystems, and ocean monitoring. For instance, it is essential for the food and chemical industries to understand the population dynamics, avoiding the rapid proliferation of algae in reservoirs or maximizing the production of species of commercial interest. It is also important for assessing water quality, with potential application to identify natural changes imparted to the environment. The salinity determination makes it possible, e.g., to calculate the water density and consequently to make estimations of pressure profiles, horizontal currents and stratification zones.

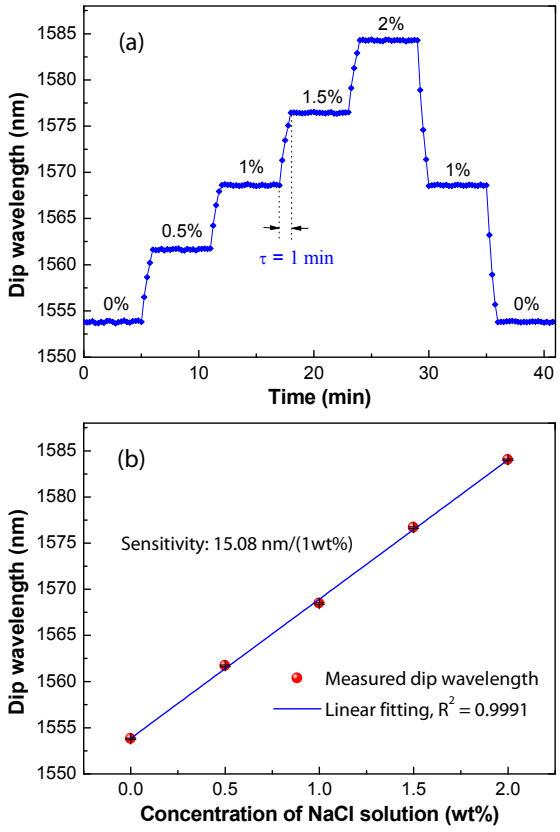

Fig. 6 Measurement of concentration of NaCl solution. (a) Real-time response of the dip wavelength with respect to change in the concentration of NaCl solution. (b) Dip wavelength as a function the concentration of NaCl solution. Error bar is standard deviation (S.D.) value

Optically measuring salinity relies on the detection of the change in refractive index of the solution. For given temperature and atmospheric pressure, the refractive index of a solution has a one-to-one correspondence with the salinity. Therefore, the salinity information can be directly determined by refractive index measurement. Here, we exploit the achieved PCF refractometer for microfluidic sensing of the concentration of NaCl solution.

Using the setup shown in fig. 4, DI water and NaCl solutions with four different concentrations were filled into the PCF in sequence. The dip wavelength was recorded at every 15 s. The experiment was performed at room temperature of 25 ºC. Fig. 6 (a) shows the real-time response of the dip wavelength with respect to the change in concentration of NaCl solution. We found that it took 1 minute for the new liquid to replace the

former liquid. Fig. 6 (b) plots the dip wavelength as a function the concentration of NaCl solution. Due to environmental perturbations (such as temperature fluctuation), the recorded dip wavelength slightly fluctuates over time. As a result, the average value of the dip wavelength during each period was applied to plot the response curve in fig. 6 (b). Through linear fitting, a sensitivity of 15.08 nm/(1wt%) with a good linearity (R^2 = 0.9991) was obtained. Then the detection limit of sensor was estimated to be 2.3×10^{-3}wt% (23 ppm).

Perspective

One unique feature of the PCF-based optofluidic sensor is the microstructured architecture and the waveguide nature of PCFs. The air hole arrangement can be flexibly designed to tailor the optical properties and the responsivity of the PCFs; and various schemes (gratings, interferometers) can be exploited for sensing applications. This helps to achieve higher sensitivity and lower detection limit. The PM-PCF used in this experiment is a commercial one (NKT Photonics), which is not particularly designed for optofluidic sensing application. Therefore, future efforts may be made to design and fabricate new PCF for such application. By optimisation of the air-hole parameters in the cross section of PCF, there is large space for enhancing the sensitivity and improving other functionalities.

Currently, we only demonstrated the salinity measurement as a proof-of-concept for the proposed refractometer. Actually, considering its high sensitivity of 8700 nm/RIU for RI around 1.333, the refractometer is also potentially attractive and useful for many other label-free optical sensing applications, such as detection of gas/vapour concentration, *in situ* bio- and chemical sensing. What's more, it is possible for one to integrate new functional materials into the microfluidic channels of the PCF to further extend its application areas. In addition, considering the miniature size of the fiber (125 μm diameter), it is also possible to embed the PCF within a microfluidic chip as the analytical part.

Conclusions

In conclusion, we have demonstrated an in-line PM-PCF-based microfluidic refractometer enabled by a C-shaped fiber, using Sagnac interferometry. The C-shaped fiber allows simultaneous in-line optical signal delivery and analyte fluid feeding to the PM-PCF. Selective exploitation of microfluidic channels of the PM-PCF was successfully achieved based on an arc discharge treatment technique. The spectral properties and the sensitivity characteristics of the fabricated refractometer were investigated theoretically and experimentally. For analyte refractive index around 1.33, it exhibits high sensitivity of 8699 nm/RIU with good linearity, which matches well with the theoretical analysis. As a proof-of-concept, we demonstrated the measurement of the concentration of NaCl solution using this refractometer. With advantages of high sensitivity, compact size, and fast response, the proposed sensor may find broad applications in the area of label-free chemical/biologic sensing.

Acknowledgements

This work is supported in part by the National Natural Science Foundation of China (11304122), in part by the Guangdong Natural Science Foundation (S2013040015234), in part by the China National Natural Science Funds for Distinguished Young Scientists (61225023), in part by the Planned Science and Technology Project of Guangzhou (2012J5100028), and in part by the Hong Kong Polytechnic University (4-ZZBE).

References

1 O. S. Wolfbeis, *Anal. Chem.*, 2008, **80**, 4269–4283.
2 X. D. Fan, I. M. White, S. I. Shopova, H. Y. Zhu, J. D. Suter, and Y. Z. Sun, *Anal. Chim. Acta*, 2008, **620**, 8-26.
3 H. Patrick, A. Kersey and F. Bucholtz, *J. Lightwave Technol.*, 1998, **16**, 1606–1612.
4 W. Liang, Y. Y. Huang, Y. Xu, R. K. Lee, and A. Yariv, *Appl. Phys. Lett.*, 2005, **86**, 151122.
5 C. F. Chan, C. Chen, A. Jafari, A. Laronche, D. J. Thomson, J. Albert, *Appl. Opt.*, 2007, **46**, 1142-1149.
6 Z. Tian, S. Yam, J. Barnes, W. Bock, P. Greig, J. M. Fraser, H. P. Loock, and R. D. Oleschuk, *IEEE Photon. Technol. Lett.*, 2008, **20**, 626-628.
7 R. Jha, J. Villatoro, G. Badenes, and V. Pruneri, *Opt. Lett.*, 2009, **34**, 617-619.
8 Q. Wu, Y. Semenova, P. Wang, and G Farrell, *Opt. Express*, 2011, **19**, 7937-7944.
9 R. C. Jorgenson and S. S. Yee, *Sens. & Actuators B - Chemical*, 1993, **12**, 213-220.
10 D. Psaltis, S. R. Quake, and C. H. Yang, *Nature*, 2006, 442, 381-386.
11 C. Monat, P. Domachuk, and B. J. Eggleton, *Nat. Photon.*, 2007, **1**, 106-114.
12 X. D. Fan and I. M. White, *Nat. Photon.*, 2011, **5**, 591-597.
13 L. Pang, H. M. Chen, L. M. Freeman, and Y. Fainman, *Lab Chip*, 2012, **12**, 3543–3551.
14 Y. Yang, A. Q. Liu, L. K. Chin, X. M. Zhang, D. P. Tsai, C. L. Lin, C. Lu, G. P. Wang, and N. I. Zheludev, *Nat. Commun.*, 2012, **3**, 651.
15 Y. Yang, L. K. Chin, J. M. Tsai, D. P. Tsai, N. Zheludev, and A. Q. Liu, *Lab Chip*, 2012, **12**, 3785–3790.
16 W. Song and D. Psaltis, *Lab Chip*, 2011, **11**, 2397–2402.
17 G. Testa and R. Bernini, *Lab Chip*, 2012, **12**, 3670–3672.
18 H. Zhu, I. M. White, J. D. Suter, M. Zourob, and X. D. Fan, *Anal. Chem.*, 2007, **79**, 930-937.
19 Y. Guo, M. K. K. Oo, K. Reddy, and X. D. Fan, *ACS Nano*, 2012, **6**, 381-388.
20 P. Domachuk, I. C. M. Littler, M. Cronin-Golomb, and B. J. Eggleton, *Appl. Phys. Lett.*, 2006, **88**, 093513.
21 P. Domachuk, C. Grillet, V. Ta'eed, E. Mägi, J. Bolger, B. J. Eggleton, L. E. Rodd, and J. Cooper-White, *Appl. Phys. Lett.*, 2005, **86**, 024103.
22 A. Crespi, Y. Gu, B. Ngamsom, H. J. W. M. Hoekstra, C. Dongre, M. Pollnau, R. Ramponi, H. H. van den Vlekkert, P. Watts, G. Cerullo and R. Osellame, *Lab Chip*, 2010, **10**, 1167–1173.

23 M. I. Lapsley, I. K. Chiang, Y. B. Zheng, X. Ding, X. Mao and T. J. Huang, *Lab Chip*, 2011, **11**, 1795–1800.
24 P. Measor, B. S. Phillips, A. Chen, A. R. Hawkins and H. Schmidt, *Lab Chip*, 2011, **11**, 899-904.
25 P. St. J. Russell, *Science*, 2003, **299**, 358-362.
26 B. J. Eggleton, C. Kerbage, P. S. Westbrook, R. S. Windeler, and A. Hale, *Opt. Express*, 2001, **9**, 698-713.
27 J. M. Fini, *Meas. Sci. Technol.*, 2004, **15**, 1120–1128.
28 B. T. Kuhlmey, B. J. Eggleton, and D. K. C. Wu, *J. Lightw. Technol.*, 2009, **27**, 1617-1630.
29 J. B. Jensen, L. H. Pedersen, P. E. Hoiby, L. B. Nielsen, T. P. Hansen, J. R. Folkenberg, J. Riishede, D. Noordegraaf, K. Nielsen, A. Carlsen, and A. Bjarklev, *Opt. Lett.*, 2004, **29**, 1974-1976.
30 T. Ritari, J. Tuominen, H. Ludvigsen, J. C. Petersen, T. Sørensen, T. P. Hansen, and H. R. Simonsen, *Opt. Express*, 2004, **12**, 4080-4087.
31 S. Konorov, A. Zheltikov, M. Scalora, *Opt. Express*, 2005, **13**, 3454.
32 J. Henningsen, J. Hald, and J. C. Petersen, *Opt. Express*, 2005, **13**, 10475.
33 A. M. Cubillas1, J. Hald, and J. C. Petersen, *Opt. Express*, 2008, **16**, 3976.
34 G. O. S. Williams, J. S. Y. Chen, T. G. Euser, P. St. J. Russell, and A. C. Jones, *Lab Chip*, 2012, **12**, 3356–3361.
35 S. Unterkofler, R. J. McQuitty, T. G. Euser, N. J. Farrer, P. J. Sadler, and P. St. J. Russell, *Opt. Lett.*, 2012, **37**, 1952-1954.
36 M. C. P. Huy, G. Laffont, V. Dewynter, P. Ferdinand, P. Roy, J. L. Auguste, D. Pagnoux, W. Blanc, and B. Dussardier, *Opt. Lett.*, 2007, **32**, 2390.
37 A. P. Zhang, G. F. Yan, S. R. Gao, S. L. He, B. K. Kim, J. Im, and Y. J. Chung, *Appl. Phys. Lett.*, 2011, **98**, 221109.
38 L. Rindorf, and O. Bang, *Opt. Lett.*, 2008, **33**, 563-565.
39 D. K. C. Wu, B. T. Kuhlmey, and B. J. Eggleton, *Opt. Lett.*, 2009, **34**, 322-324.
40 J. Villatoro, M. P. Kreuzer, R. Jha, V. P. Minkovich, V. Finazzi, G. Badenes, and V. Pruneri, *Opt. Express*, 2009, **17**, 1447–1453.
41 A. Amezcua-Correa, J. Yang, C. E. Finlayson, A. C. Peacock, J. R. Hayes, P. J. A. Sazio, J. J. Baumberg, and S. M. Howdle, *Adv. Funct. Mater.*, 2007, **17**, 2024–2030.
42 C. M. B. Cordeiro, C. J. S. de Matos, E. M. dos Santos, A. Bozolan, J. S. K. Ong, T. Facincani, G. Chesini, A. R Vaz and C. H. B. Cruz, *Meas. Sci. Technol.*, 2007, **18**, 3075-3081.
43 A. Brakel, C. Grivas, M. N. Petrovich, and D. J. Richardson, *Opt. Express*, 2007, **15**, 8731.
44 H. Lehmann, H. Bartelt, R. Willsch, R. Amézcua-Correa, and J. C. Knight, *IEEE Sens. J.*, 2011, **11**, 2926.
45 C. Wu, M. L. V. Tse, Z. Liu, B. O. Guan, Chao Lu, and H. Y. Tam, *Opt. Lett.*, 2013, **38**, 3283.
46 L. M. Xiao, M. S. Demokan, W. Jin, Y. Wang, C. L. Zhao, *J. Lightw. Technol.*, 2007, **25**, 3563.
47 M. L. V. Tse, H. Y. Tam, L. B. Fu, B. K. Thomas, L. Dong, C. Lu, and P. K. A. Wai, *IEEE Photon. Technol. Lett.*, 2009, **21**, 164.
48 Y. Liu, B. Liu, X. Feng, W. Zhang, G. Zhou, S. Yuan, G. Kai, and X. Dong, *Appl. Opt.*, 2005, **44**, 2382.
49 A. H. Harvey, J. S. Gallagher, and J. M. Sengers, *J. Phys. Chem. Ref. Data*, 1998, **27**, 761.
50 K. Nielsen, D. Noordegraaf, T. Sørensen, A. Bjarklev, and T. P. Hansen, *J. Opt. A*, 2005, **7**, L13-L20.
51 X. Dong, H. Y. Tam, P. Shum, *Appl. Phys. Lett.*, 2007, **90**, 151113.
52 I. M. White and X. D. Fan, *Opt. Express*, 2008, **16**, 1020.